Applied Catalysis B: Environmental 325 (2023) 122336

Contents lists available at ScienceDirect

Applied Catalysis B: Environmental

journal homepage: www.elsevier.com/locate/apcatb

Chlorophyll-modified $Au_{25}(SR)_{18}$-functionalized TiO_2 for photocatalytic degradation of rhodamine B

Thanaree Phongamwong [a,b], Noelia Barrabés [c], Waleeporn Donphai [a,b], Thongthai Witoon [a,b], Günther Rupprechter [c,*], Metta Chareonpanich [a,b,**]

[a] KU-Green Catalysts Group, Department of Chemical Engineering, Faculty of Engineering, Kasetsart University, Bangkok 10900, Thailand
[b] Center for Advanced Studies in Nanotechnology for Chemical, Food and Agricultural Industries, KU Institute for Advanced Studies, Kasetsart University, Bangkok 10900, Thailand
[c] Institute of Materials Chemistry, Technische Universität Wien, Getreidemarkt 9/BC/01, Vienna 1060, Austria

ARTICLE INFO

Keywords:
Photocatalysis
Au_{25} clusters
Chlorophyll
RhB degradation
Visible light

ABSTRACT

Solar-driven photocatalysis is a promising route toward cleaner production using sunlight as a sustainable energy source. Nanocrystalline TiO_2, in the form of mixed anatase/rutile phases (P25), is often employed, but must be modified for higher activity in visible light. To improve the light harvesting properties, nano-bio hybrid photocatalysts were prepared by functionalizing P25 with Au_{25} clusters, Au nanoparticles, and/or chlorophyll. The most effective photocatalytic degradation of rhodamine B (RhB) was observed over P25 catalysts functionalized with both Au_{25} and chlorophyll. HR-TEM, UV–vis, XPS and XANES/EXAFS were applied to examine the factors influencing photocatalytic activity. A direct contact between Au_{25}, chlorophyll, and P25, strongly improved the electron transfer from chlorophyll to P25, while still maintaining the reusability of catalysts. For chlorophyll-modified $Au_{25}(SR)_{18}$-functionalized P25 catalyst, the degradation rate of RhB was enhanced ~16 times compared to that of P25.

1. Introduction

Photocatalytic reactions using solar light as an energy source are considered as a promising route for the removal of harmful contaminants from wastewater effluents. Nanocrystalline TiO_2 based on mixed anatase/rutile phases (P25) has been widely applied as photocatalyst. However, due to its large band gap (3.2 eV), the use of visible light is not practical. In our previous studies, chlorophyll has thus been deposited on TiO_2 to improve the light harvesting properties. Using Mg-stabilized chlorophyll, the photocatalytic degradation rate of rhodamine B (RhB) doubled [1–3]. Herein, for further surface functional modification of TiO_2 we additionally added Au clusters and Au nanoparticles (NPs), again with chlorophyll loading, leading to improved photocatalytic performance. This creates nano-bio hybrid photocatalysts, which have been systematically explored.

To date, TiO_2 supported Au nanoparticles (NPs) larger than 3 nanometers, which have a bulk-like electronic band structure, have been extensively applied in photocatalytic processes as their surface plasmon resonance (SPR) enables to efficiently absorb visible light [4–6]. Nevertheless, the photon yield of Au NPs is low due to ultrafast relaxation of the hot electrons via electron-hole pair recombination [7,8]. In contrast, Au particles smaller than 2 nm, i.e., nanoclusters, exhibit a discontinuous electronic structure, so that quantum confinement effects may dominate. Due to the discrete energy levels, the excited electrons in Au nanoclusters have longer lifetime, making clusters promising photosensitizers [9,10]. However, such small clusters may suffer from structure instability [11,12]. Consequently, thiolate-protected Au nanoclusters are an alternative to conventional Au nanoparticles as their exact size (number of Au atoms), atomic structure, and ligand shell can be precisely tuned and controlled at the atomic level [12–16]. Among these, $Au_{25}(SC_2H_4Ph)_{18}$ or $Au_{25}(SR)_{18}$ (R = $-CH_2-CH_2-C_5H_6$) with a core-shell structure (different from the face-centered cubic structure of larger bulk gold NPs) is one of the most stable ligand–protected Au nanoclusters and has been frequently applied for (thermo)catalytic studies [17–21]. The core of $Au_{25}(SR)_{18}$ cluster is formed by 13 inner Au atoms, with one central Au atom being surrounded by a Au_{12}

* Corresponding author.
** Corresponding author at: KU-Green Catalysts Group, Department of Chemical Engineering, Faculty of Engineering, Kasetsart University, Bangkok 10900, Thailand.
E-mail addresses: guenther.rupprechter@tuwien.ac.at (G. Rupprechter), fengmtc@ku.ac.th (M. Chareonpanich).

https://doi.org/10.1016/j.apcatb.2022.122336
Received 31 October 2022; Received in revised form 25 December 2022; Accepted 27 December 2022
Available online 28 December 2022

icosahedron, stabilized by six –S-Au-S-Au-S- motifs, called long staples, located on different faces of the icosahedron. The absorption spectra of Au_{25} nanoclusters display characteristic features resulting from electronic transitions between the different molecular orbitals. Thus, the combined light harvesting capability and catalytic activity of Au_{25} nanoclusters should be very beneficial for photocatalytic reactions, i.e., dye degradation.

Indeed, P25 modified with Au_{25} clusters and chlorophyll showed the highest efficiency in the photocatalytic degradation of RhB. Proper functionalization of $Au_{25}(SR)_{18}$ and chlorophyll increased the photocatalytic activity of P25 by approximately 3.6 times. Detailed characterization of the atomic, electronic, and optical characteristics of the modified photocatalysts by a range of methods (see below) enabled to clarify structure-reactivity-relationships.

2. Experimental

2.1. Preparation of chlorophyll-modified Au-functionalized TiO_2 (P25) photocatalysts

To functionalize P25 TiO_2 with Au nanoclusters and Au nanoparticles, as well as with chlorophyll, several modification routes were applied. In all cases, the loading amounts of Au and chlorophyll were fixed at 0.5 wt% each.

2.1.1. Preparation of $Au_{25}(SR)_{18}$ nanoclusters on P25

The thiolate-protected gold clusters, $Au_{25}(SR)_{18}$, were prepared following procedures as reported by García et al. [20,22] and Rupprechter [21] (and references therein). Consequently, 50 ml of tetrahydrofuran (THF, $(CH_2)_3CH_2O$) was added to 500 mg tetrachloroauric (III) acid trihydrate ($HAuCl_4 \bullet 3\ H_2O$) mixed with 1.2 equiv. of tetraoctylammonium bromide (TOAB, $C_{32}H_{68}BrN$) under stirring at 300 rpm for 20 min. Subsequently, 5 equiv. of 2-phenylethanethiol ($C_8H_{10}S$) was added dropwise to the obtained mixture until the solution turned transparent. Next, 10 ml ice cold water containing 10 equiv. of $NaBH_4$ was quickly added to the mixture and kept stirring at room temperature for 4 days. After that, the THF solvent was removed by a rotary evaporator and the remaining solution was washed with 75/25 mixture of ethanol/milli-Q water. The synthesized $Au_{25}(SR)_{18}$ clusters were then extracted from excess thiol using THF and were characterized by UV–vis spectroscopy (Fig. S1). Three characteristic absorption bands around 400, 450 and 670 nm confirmed that $Au_{25}(SR)_{18}$ clusters was successfully synthesized [22–24], with a cluster size of approximately 1.4 nm.

Next, the required mass of $Au_{25}(SR)_{18}$ nanoclusters (to obtain 0.5 wt % Au loading) was dissolved in dichloromethane and 1 g of P25 powder was added. After stirring for 24 h, the catalyst was collected by filtration, dried at 60 °C, and calcined in air at 400 °C for 1 h to remove the thiolate ligands (catalyst denoted as Au_{25}/P25). The dried catalyst with intact thiolate ligands was used for comparison, denoted as Au_{25}/P25 (uc) (uc = uncalcined).

2.1.2. Loading of Au/P25 by deposition-precipitation

As a benchmark photocatalyst, 0.5 wt% Au on P25 was prepared by deposition-precipitation (DP), as reported by Zhang et al. [25]. In this case, 96 ml of milli-Q water was added to P25, then 4.4 ml of 0.03 M of $HAuCl_4$ solution was added dropwise to the suspension, while 0.1 M Na_2CO_3 solution was added to maintain pH at 7 under stirring. After that, the mixture was heated to 70 °C for 1 h. The photocatalyst was collected by filtration, dried at 100 °C for 12 h, and calcined at 400 °C for 1 h. As shown below, the Au particle size was approximately 2 nm. The obtained catalyst was denoted as Au_{DP}/P25.

2.1.3. Preparation of larger Au nanoparticles on P25

To examine size effects, larger Au nanoparticles (Au NPs) were prepared by the citrate method. Following the work reported by Wang et al. [26], 1 ml of 1% w/v $HAuCl_4$ solution was added to 100 ml ice water and then 1 ml of 1% w/v trisodium citrate ($C_6H_5Na_3O_7$) was added to the solution under vigorous stirring for 1 min. After that, 1 ml of a freshly prepared 0.075% w/v sodium borohydride ($NaBH_4$) solution was added to initiate reduction. The color of the solution then rapidly changed from yellow to ruby-red, indicating the formation of Au nanoparticles. The Au particle size was calculated based the optical absorption spectra (UV–vis; Fig. S1), as described by Haiss et al. [27], yielding Au NPs with a mean particle size of ~6.0 nm (denoted as $Au_{6\ nm}$/P25).

Furthermore, even larger Au NPs were prepared by a simple citrate method [28]. Thus, 500 ml of 0.25 mM $HAuCl_4$ aqueous solution was boiled at 100 °C under stirring. Then 12.5 ml of 0.03 M sodium citrate solution was added, and the obtained solution was boiled at 100 °C for 15 min. After that, the solution was left to cool to room temperature, and Au NPs in wine-red solution were obtained. The size of Au NPs, calculated based on UV–vis (Fig. S1), was found to be ~17.4 nm (denoted as $Au_{17\ nm}$/P25).

Again, a defined mass of Au nanoparticles was dissolved in water and 1 g of P25 powder was added. After stirring for 24 h, each catalyst was collected by filtration and dried at 60 °C.

2.1.4. Chlorophyll loading onto Au-functionalized P25 photocatalysts

Chlorophyll was extracted from dried *Spirulina* using methanol following a previously reported procedure [1]. The extracted chlorophyll *a* solution with proper of 0.5 wt% loading was then added to the obtained Au-functionalized P25 catalysts by incipient wetness impregnation, with the mixture stirred at room temperature for 12 h. After that, the chlorophyll- (Chl-) loaded catalysts were collected by removing the solvent using a rotary evaporator: labeled as Chl/P25, Chl-Au_{25}/P25 (uc), and Chl-Au_{25}/P25. The amount of chlorophyll *a* was calculated using Eq. (1) reported by Bennett and Bogorad [29].

$$\text{Chlorophyll a} = 13{\cdot}9A_{665}\ (\text{mg/l}) \quad (1)$$

where A_{665} is the absorbance at 665 nm measured by a UV–vis spectrophotometer.

2.2. Characterization of functionalized P25 photocatalysts

X-ray diffraction (XRD) measurements were carried out at room temperature by using a Philips X′Pert diffractometer operated with Cu-Kα radiation (0.154 nm) in Bragg-Brentano reflection geometry, yielding the catalyst crystal structure. The scanning range was 10–90° in step scan mode of 0.02°. The crystallite sizes were analyzed via the Scherrer equation.

N_2 adsorption-desorption isotherms of catalysts were recorded at –196 ℃ using a Quantachrome Autosorp-1 C instrument. The specific surface areas were obtained from Brunauer–Emmett–Teller (BET) analysis, with pore size distributions being analyzed by using the Barrett–Joyner–Halenda (BJH) method. The specific pore volumes were measured at a relative P/P_0 of 0.995.

High-angle annular dark-field scanning transmission electron microscopy (HAADF-STEM) was applied to determine the particle size and size distribution of Au clusters and NPs. For high resolution (HR-TEM) imaging, all the samples were also characterized by field emission transmission electron microscopy (FETEM: JEOL, JEM-3100 F) at 300 kV acceleration voltage using the bright field (BF) mode.

The functional groups of the functionalized photocatalysts were identified by Fourier transform infrared spectroscopy (FTIR: PerkinElmer, Frontier) in the range 4000–400 cm^{-1}.

X-ray photoelectron spectroscopy (XPS), carried out at beamline 3.2a of the Synchrotron Light Research Institute (SLRI), Thailand, was used to identify the oxidation state and atomic concentration of Au on the catalyst surface. The photoelectron spectra were collected by a Thermo VG Scientific Alpha110 energy analyzer in energy steps of 0.1 eV. The C 1 s peak at 284.6 eV was used as binding energy reference.

Table 1
Specific surface area, total pore volume, average pore size, and band gap of P25 and functionalized P25 catalysts.

Catalysts	Specific surface area (m^2/g)	Total pore volume (cm^3/g)	Average pore size (nm)	Surface concentration[a] (at%)	Band gap (eV)
P25	65	0.38	23.6	n/a	3.10
Au_{25}/P25 (uc)	59	0.67	45.7	0.12	3.07
Au_{25}/P25	52	0.79	60.9	0.08	3.04
Au_{DP}/P25	55	0.56	40.9	0.29	2.82
$Au_{6\ nm}$/P25	55	0.57	41.4	0.17	2.88
$Au_{17\ nm}$/P25	60	0.56	37.5	n/a	2.90
Chl/P25	46	0.49	42.9	n/a	2.86
Chl-Au_{25}/P25 (uc)	37	0.59	64.2	0.17	2.89
Chl-Au_{25}/P25	38	0.68	72.6	0.15	3.01

[a] Calculated from XPS analysis.
n/a: Not applicable.

The electronic states of Au in the catalysts were examined by X-ray absorption near edge structure (XANES) at Beamline 1.1 of the SLRI, Thailand. Au L3-edge spectra were recorded at room temperature in transmission mode, with gold foil used for calibration (E_0 of 11919 eV). The obtained spectra were analyzed using the Athena program. Extended X-ray absorption fine structure (EXAFS) was also performed to investigate the local structure of supported Au_{25} clusters. For data fitting, the procedure was performed on the k_2-weighted from 3 to 8 $Å^{-1}$.

UV–vis diffuse reflectance spectroscopy (UV–vis DRS: PerkinElmer, Lambda 750) was performed to observe optical properties of the photocatalysts, using $BaSO_4$ as a reflectance reference. The band gap energy of the photocatalysts was calculated using the Kubelka–Munk function.

Photoluminescence spectroscopy (PL: AvaSpec-2048TEC, Avantes) was performed using an excitation wavelength of 255 nm in the range of 300–700 nm to examine charge transfer processes of the photocatalysts.

2.3. Degradation of rhodamine B over chlorophyll-modified Au-functionalized P25 photocatalysts

Prior to each experiment, the capacity of the photocatalysts to adsorb RhB ($C_{28}H_{31}ClN_2O_3$: HIMEDIA, practical grade) at room temperature in the dark was determined. The photocatalysts (30 mg) were suspended in 30 ml of RhB aqueous solution (30 mg/L) in a glass tube reactor, applying a magnetic stirrer for 30 min. After reaching equilibrium, the absorption of the remaining RhB solution at a wavelength around 554

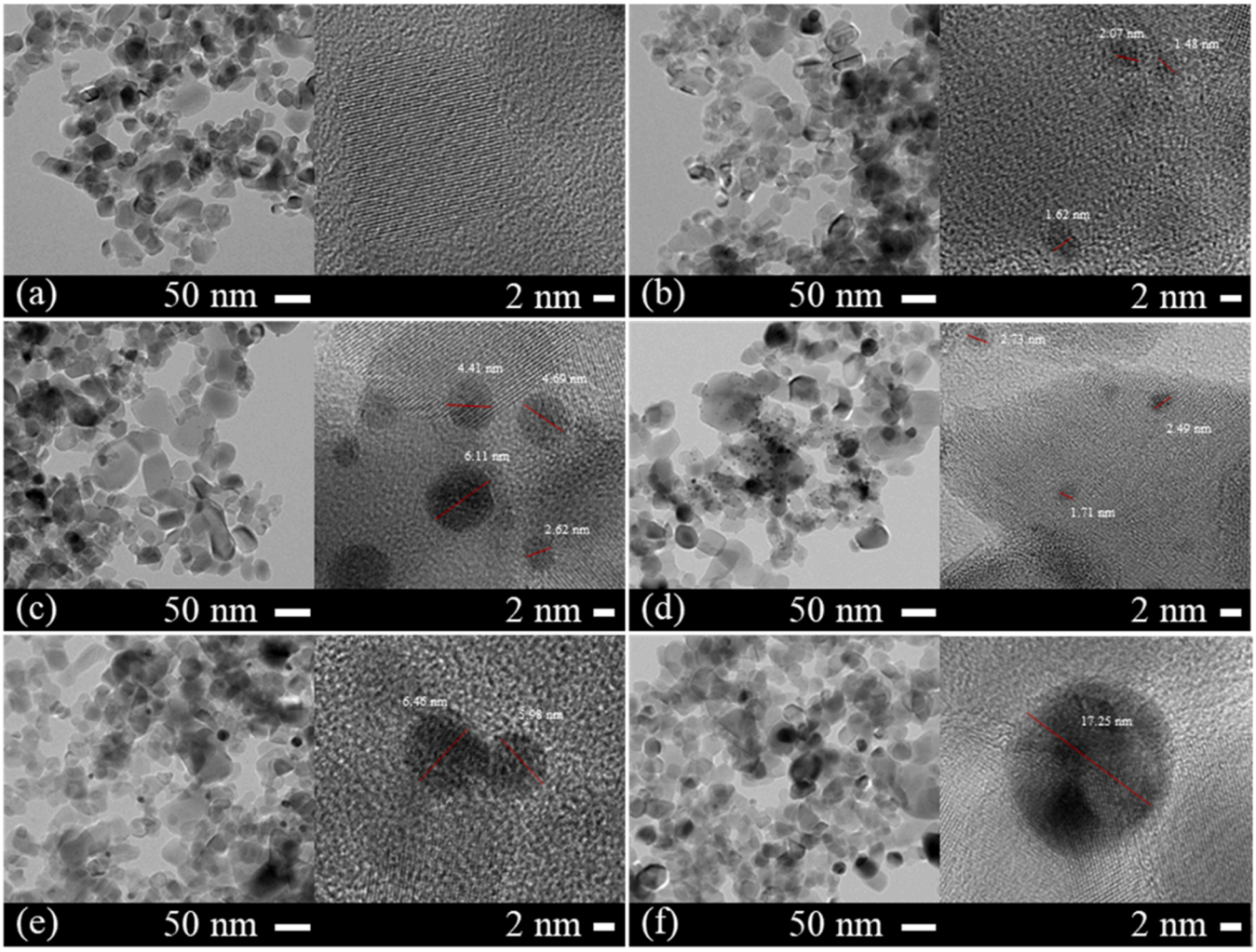

Fig. 1. HR-TEM images of (a) P25 and Au-functionalized photocatalysts: (b) Au_{25}/P25 (uc), (c) Au_{25}/P25, (d) Au_{DP}/P25, (e) $Au_{6\ nm}$/P25, and (f) $Au_{17\ nm}$/P25 catalysts.

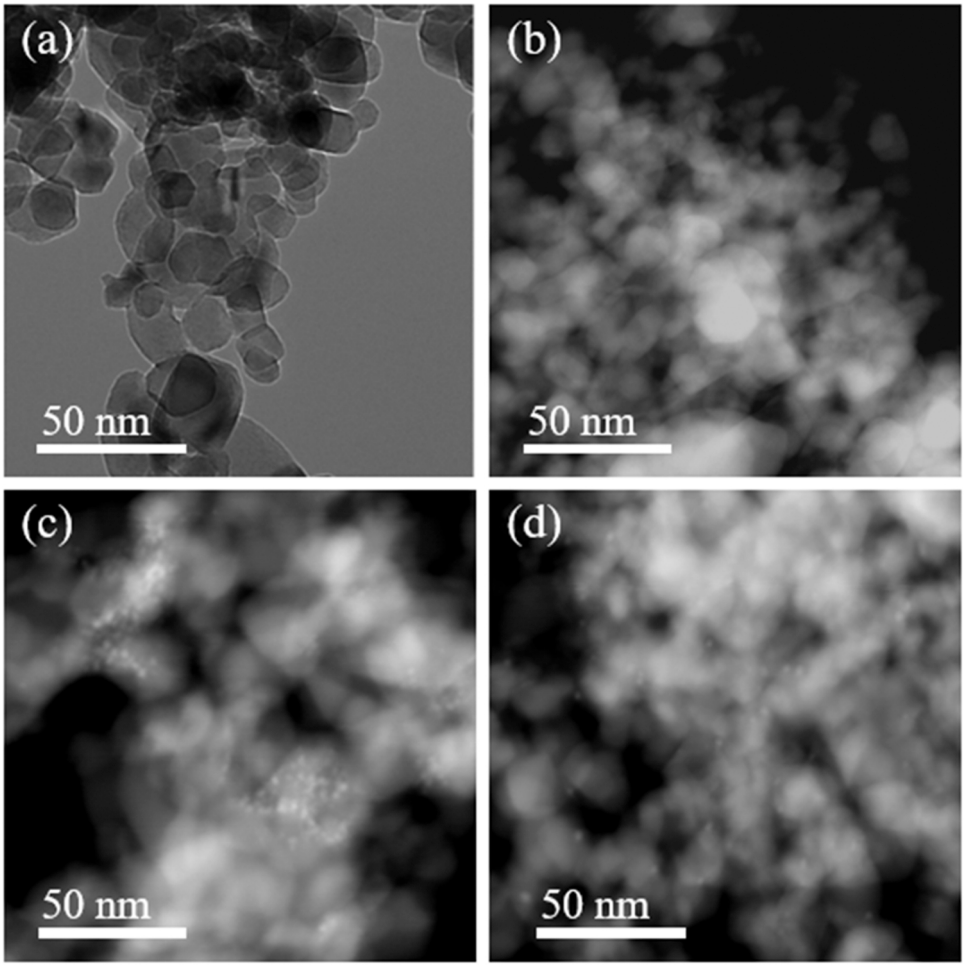

Fig. 2. STEM images of chlorophyll-modified Au-functionalized photocatalysts: (a,b) Chl/P25, (c) Chl-Au_{25}/P25 (uc), and (d) Chl-Au_{25}/P25 catalysts.

nm was measured by UV–vis (Thermo Scientific, Genesys 10 series).

The photocatalytic performance of the catalysts in RhB degradation was then evaluated by the following procedure: Under dark conditions, oxygen gas was introduced into the mixture of catalyst (30 mg) and 30 ml RhB solution for 30 min. At equilibrium, the concentration of RhB was measured and used as an initial concentration (C_0). After that, two 50 W LED floodlights (TEMTOP) located at opposite sides of the reactor were turned on, starting the room temperature photocatalytic degradation reaction. After specific times, the residual concentration of RhB was measured by UV–vis.

The kinetic rates (k) of RhB photodegradation over modified P25 catalysts were calculated using a pseudo-first-order kinetic equation [30–32]:

$$\ln(C_0/C) = kt \quad (2)$$

where C_0 and C (mg/L) are RhB concentrations at initial and time t, respectively; k (min^{-1}) is the pseudo-first-order kinetic rate constant; and t (min) is the irradiation time.

3. Results and discussion

3.1. Textural and structural properties of chlorophyll-modified Au-functionalized TiO_2

BET analysis (Fig. S2) showed a type IV isotherm with hysteresis loop for all catalysts [33]. This indicated that loading P25 with Au_{25} clusters, Au nanoparticles, and/or chlorophyll did not alter the mesoporous structure of P25. As shown in Fig. S2 and Table 1, the specific surface area of P25 (65 m^2/g) was slightly reduced upon Au loadings, but significantly reduced upon chlorophyll loading (37 m^2/g). The latter suggested partial blockage of P25 due to chlorophyll loading.

The XRD patterns of all photocatalysts exhibited only peaks characteristic of anatase and rutile TiO_2 phases (approximately 75% and 25%, with 22 and 78 nm average crystallite size, respectively; Fig. S3). It should be noted that no diffraction peaks of Au were detected due to peak broadening caused by relatively small sizes of Au_{25} and Au nanoparticles, and the low Au loading [34,35].

Fig. 1 shows HR-TEM images of P25 and Au-functionalized P25, obtained by FETEM in bright field (BF) mode. All images (Fig. 1b–f) displayed rather spherical shapes of gold nanoparticles, imaged as darker spots. The Au_{25} clusters in the Au_{25}/P25 (uc) sample (Fig. 1b) exhibited a homogeneous and uniform distribution of Au nanoparticles on P25 with an average Au cluster size of 1.4 nm, agreeing with that reported by Li et al. [36], Lopez-Acevedo et al. [37], and Li et al. [14]. As shown in Fig. 1c, the calcined (ligand-free) Au_{25}/P25 had larger Au cluster size (approximately 4.5 nm). This may be attributed to partial agglomeration of Au nanoparticles upon ligand removal, as also reported by Li et al. [36] and Gaur et al. [38].

The average Au cluster size of Au_{DP}/P25 (Fig. 1d) was 2.3 nm, while those of the (citrate) $Au_{6\ nm}$/P25 and $Au_{17\ nm}$/P25 (Fig. 1e and f) were 6.2 and 17.2 nm, respectively. These results are in good agreement with the corresponding Au cluster sizes calculated from UV–vis spectra (as shown in Fig. S1).

Furthermore, STEM results indicated that adding chlorophyll did not significantly affect the Au_{25} cluster size, as the average sizes of Au_{25} in Chl-Au_{25}/P25 (uc) and Chl-Au_{25}/P25 catalysts (Fig. 2c and d) were still

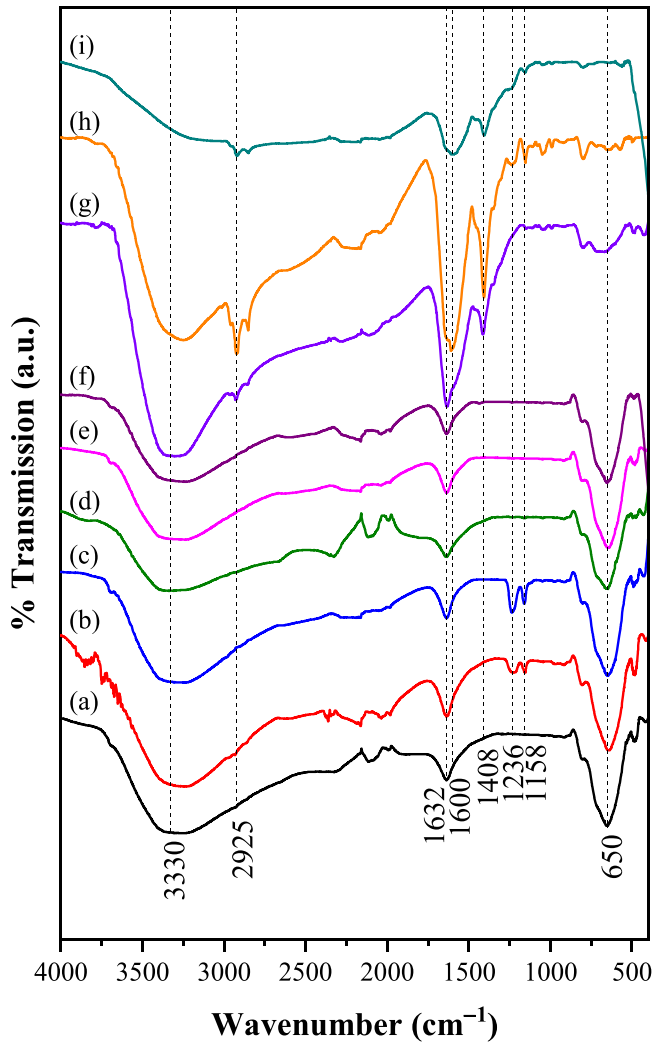

Fig. 3. FT-IR spectra of (a) P25, (b) Au_{25}/P25 (uc), (c) Au_{25}/P25, (d) Au_{DP}/P25, (e) $Au_{6\ nm}$/P25, (f) $Au_{17\ nm}$/P25, (g) Chl/P25, (h) Chl-Au_{25}/P25 (uc), and (i) Chl-Au_{25}/P25 catalysts.

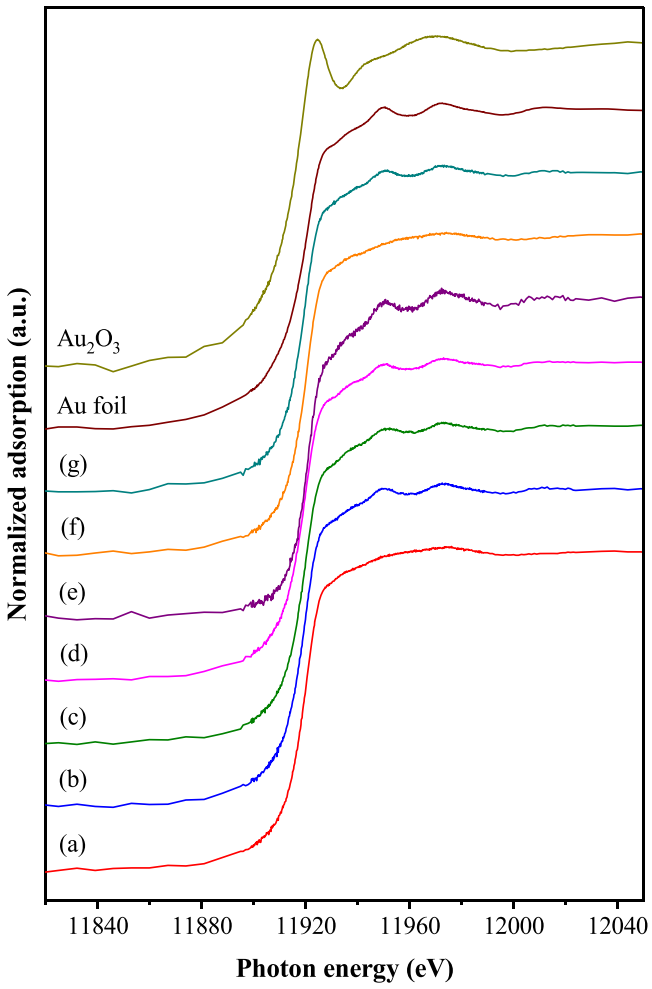

Fig. 4. Normalized Au L_3-edge XANES spectra of reference compounds (Au foil and Au_2O_3) and functionalized P25 catalysts: (a) Au_{25}/P25 (uc), (b) Au_{25}/P25, (c) Au_{DP}/P25, (d) $Au_{6\ nm}$/P25, (e) $Au_{17\ nm}$/P25, (f) Chl-Au_{25}/P25 (uc), and (g) Chl-Au_{25}/P25 catalysts.

1.9 and 3.9 nm, respectively.

FTIR spectra of P25 and modified P25 catalysts (Fig. 3) revealed the characteristics of functional groups present in all photocatalysts. The bands around 3330 and 1632 cm^{-1} represented the O–H stretching and bending vibrations of Ti–OH of P25, respectively. After Au_{25} loading, peaks at 1236 and 1158 cm^{-1} indicating the C–C stretching modes of thiol ligands were detected for both Au_{25}/P25 (uc) and Au_{25}/P25 catalysts (Fig. 3b and c). However, only Au_{25}/P25 (uc) showed weak peaks of aromatic and aliphatic C–H stretching modes at 2933 and 2866 cm^{-1} of fully intact thiol ligands (Fig. 3b) [39]. This confirmed the intact ligands on Au_{25} clusters in the Au_{25}/P25 (uc) catalyst, and the partial removal of thiol ligands in Au_{25}/P25.

For chlorophyll-loaded catalysts (Fig. 3g–i), the presence of chlorophyll on the catalyst surface was confirmed by peaks around 2925, 1600, and 1408 cm^{-1}, originating from the C–H stretching of methyl, methylene or methine groups, C═O stretching in conjugated ketone and carbonyl groups, and C═N stretching in chlorophyll, respectively [40,41]. A peak around 650 cm^{-1}, corresponding to the Ti–O–Ti stretching vibration, found for P25 and all Au/P25 catalysts, was much weaker in the chlorophyll-modified catalysts, indicating that chlorophyll covered large fractions of the P25 surface.

3.2. Characterization of electronic properties of chlorophyll-modified Au-functionalized TiO_2

To investigate the electronic states and local structure of the photocatalysts, XANES measurements were performed at the Au L_3-edge. As shown in Fig. 4, XANES spectra of all catalysts exhibited a white line intensity and edge energy similar to those of the Au foil reference, indicating that in the calcined catalysts Au was metallic (Au^0). Moreover, the white line intensities of Au in the uncalcined catalysts (Au_{25}/P25 (uc) and Chl-Au_{25}/P25 (uc)) were slightly lower than that of the Au foil. This may be due to the presence of the thiolate ligands (Au–S bonds), leading to partial oxidation of Au atoms [42]. However, most of the Au atoms in $Au_{25}(SR)_{18}$ were still metallic.

In addition, the R-space of EXAFS spectra of the Chl-Au_{25}/P25 (uc) and Chl-Au_{25}/P25 catalysts (Fig. S4) confirmed the different structures of Au_{25} in the uncalcined and calcined catalysts, related to the partial removal of thiol ligands upon calcination [15]. For Chl-Au_{25}/P25 (uc), a peak at the bond distance around 2 Å was attributed to the Au–S bond, whereas a small peak above 2 Å was related to the Au–Au bonds in $Au_{25}(SR)_{18}$ clusters [42,43]. After calcination at 400 °C for 1 h, the thiolate ligands were partially removed from the Au_{25} clusters, as evident from the significant decrease in the Au–S bond in the respective Chl-Au_{25}/P25 spectrum.

The electronic properties of Au in the series of chlorophyll-modified Au-functionalized catalysts were further examined by XPS (Fig. S5),

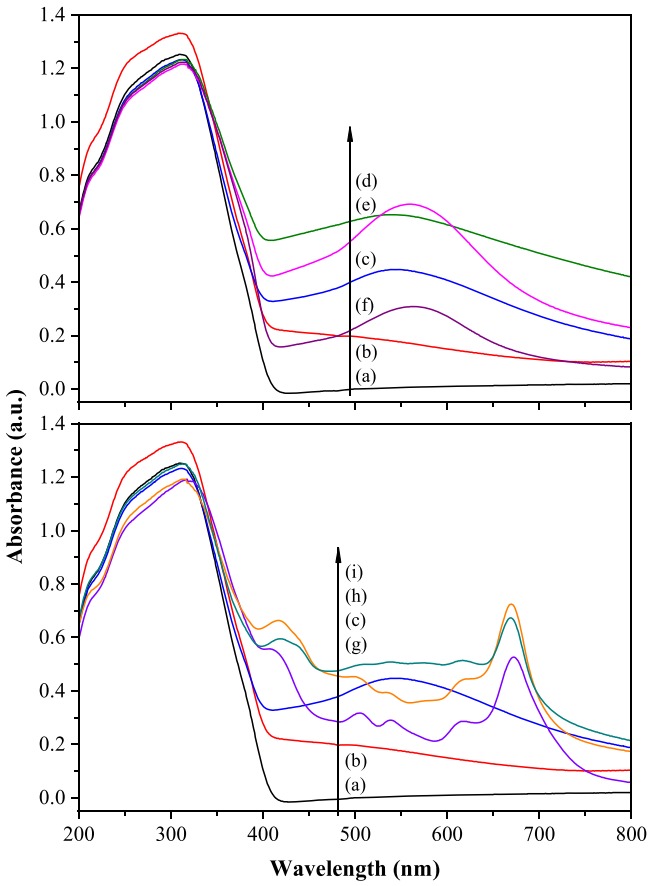

Fig. 5. UV–vis diffuse reflectance spectra of (a) P25, (b) Au_{25}/P25 (uc), (c) Au_{25}/P25, (d) Au_{DP}/P25, (e) $Au_{6\ nm}$/P25, (f) $Au_{17\ nm}$/P25, (g) Chl/P25, (h) Chl-Au_{25}/P25 (uc), and (i) Chl-Au_{25}/P25 catalysts.

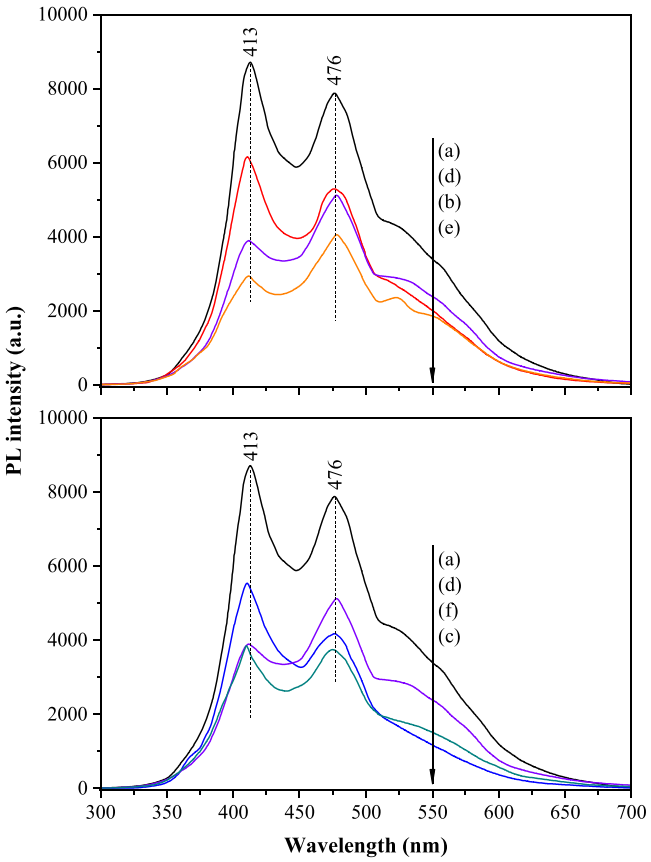

Fig. 6. PL spectra of P25 and functionalized P25 catalysts (excitation at 255 nm): (a) P25, (b) Au_{25}/P25 (uc), (c) Au_{25}/P25, (d) Chl/P25, (e) Chl-Au_{25}/P25 (uc), and (f) Chl-Au_{25}/P25 catalysts.

although the signals were quite weak due to the low Au loading. Nevertheless, the spectra are very surface sensitive, as for a kinetic energy of ~500 eV, the inelastic mean free path (IMFP) of the photoelectrons is ~1 nm. The Au surface concentration in the catalysts based on the XPS analysis was in a range of 0.08–0.29 at% Au.

Regarding Au_{25}/P25 (uc) catalyst, the Au 4 $f_{7/2}$ and 4 $f_{5/2}$ peaks with binding energies of ~83.4 and ~86.8 eV, respectively, were attributed to metallic Au in the core and to a lesser extent to Au(I) in the staples, due to the presence of thiolate ligands [20,22]. This is in good agreement with the EXAFS results and previous reports of Au(0)@Au(I)-thiolate "core-shell" nanostructures [44,45]. In the case of the calcined Au_{25}/P25 catalyst, the Au 4 f binding energies shifted to lower values around ~82.2 eV and ~85.7 eV, corresponding to metallic Au and reflecting the ligand removal [15,16,21]. The shift in the binding energy of Au_{25}/P25 may also originate from Au agglomeration upon ligand removal during calcination, leading to larger Au cluster sizes (approximately 4.5 nm vs. 1.4 nm for Au_{25}/P25 (uc)) [46,47].

For Au_{DP} and $Au_{6\ nm}$, metallic Au was observed, with the ~2.5 nm particles in Au_{DP} leading to higher binding energies. Signals were too low for $Au_{17\ nm}$/P25 catalyst, due to the large particle size and thus low Au dispersion. In the case of Chl-Au_{25}/P25 (uc) and Chl-Au_{25}/P25, only small further binding energy shifts were observed upon chlorophyll loading.

3.3. *Visible-light absorption of chlorophyll-modified Au-functionalized TiO_2*

As efficient light harvesting is of crucial importance for photocatalysts, Fig. 5 shows corresponding absorption spectra. The P25 catalyst (Fig. 5a) exhibited an absorption peak only in the UV region (< 400 nm) due to the intrinsic absorption and high energy band gap of TiO_2. After Au loading, Au/P25 catalysts (Fig. 5b–f) showed a red shift and an increase in the visible light absorbance.

For Au NPs-functionalized P25 catalysts (Au_{DP}/P25, $Au_{6\ nm}$/P25, $Au_{17\ nm}$/P25: Fig. 5d–f), the enhancement of visible-light absorbance mainly originated from a broad band centered around 540–565 nm, attributed to a localized surface plasmon resonance (LSPR) of the Au nanoparticles [48–52]. It originates from an oscillation of excited electrons in the conduction band of the Au 6 *s* orbital and frequently occurs for Au particles between 5 and 50 nm [52]. The absorption band position and width depend on the confinement of electrons within the dispersed Au nanoparticles [49]. As can be seen in Fig. 5, a red shift of the absorption band occurred upon increasing the Au particle size [53,54].

For Au_{25}-functionalized P25 catalysts (Fig. 5b and c), the Au_{25}/P25 (uc) catalyst exhibited higher visible-light absorption than P25. In addition, the calcined Au_{25}/P25 catalyst had an absorption band at ~540 nm, resulting from the LSPR effect of the agglomerated Au clusters, in agreement with the TEM analysis (Fig. 1).

Upon chlorophyll loading (Fig. 5g–i), a further increase in visible-light absorption (400–800 nm) was found, originating from chlorophyll *a* (absorption spectra of extracted chlorophyll are shown in Fig. S6) [1]. The visible-light absorption of Chl-Au_{25}/P25 (uc) and Chl-Au_{25}/P25 catalysts was significantly stronger than that of catalysts loaded by either Au_{25} or chlorophyll. This suggested that the presence of both Au_{25} and chlorophyll helped improving the visible-light absorption.

The band gap energies of all photocatalysts were calculated from the Kubelka–Munk function (Fig. S7) and are listed in Table 1. Functionalizing P25 by Au_{25} and Au NPs narrows the band gap of photocatalysts

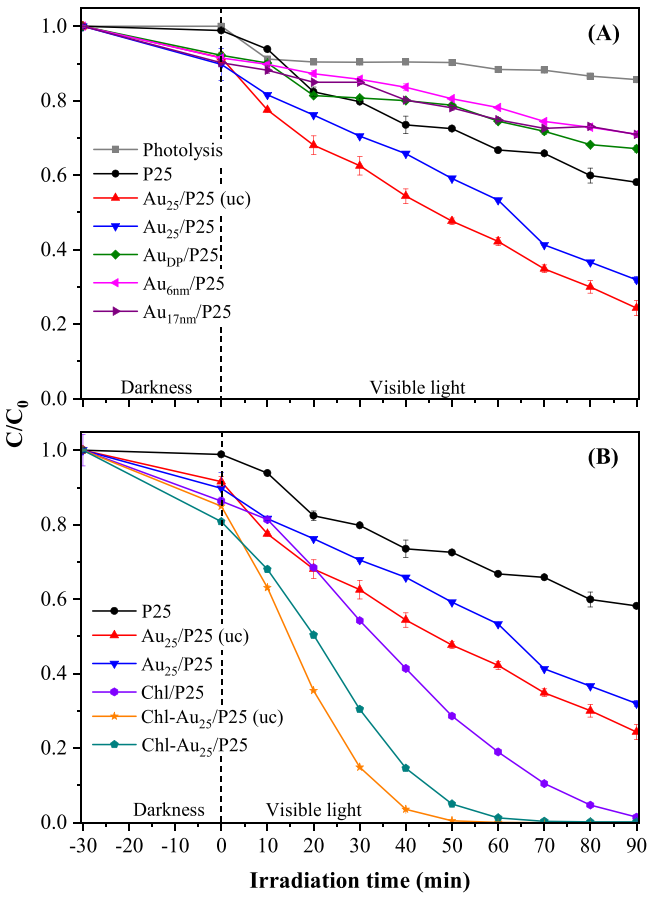

Fig. 7. Photocatalytic degradation of rhodamine B over P25 and functionalized P25 catalysts.

due to strong interaction between Au and P25, as reported by Rosseler et al. [52] and Kmetykó et al. [53]. Modification by chlorophyll then further decreased the band gap of the catalysts. As a result, chlorophyll modified Au_{25}-functionalized P25 (Chl-Au_{25}/P25 (uc) and Chl-Au_{25}/P25) catalysts exhibited outstanding absorption properties.

3.4. Charge and energy transfer between P25, Au and chlorophyll

Photoluminescence (PL) emission originates from the undesired recombination of electron-hole pairs [7,55]. Consequently, limiting the recombination of photogenerated charges (electron-hole pairs) is another key asset of effective photocatalysts. To examine charge transfer and charge separation of the catalysts, PL spectra were measured at an excitation wavelength of 255 nm (Fig. 6 and Fig. S8).

For Au_{25}-loaded catalysts, the reduction in PL intensity is due to electron transfer from Au_{25} clusters to the TiO_2 conduction band. Consequently, photogenerated electron-hole pairs can be effectively separated on Au_{25}/P25 catalysts, resulting in a prolonged lifetime of the photogenerated charge carriers, thus improving the photocatalytic activity. All Au functionalized P25 catalysts exhibited lower PL intensities than P25, specifically for Au_{DP}/P25 and $Au_{6\ nm}$/P25. For $Au_{17\ nm}$/P25 catalyst, the large Au particle size (17.4 nm) was reported to reduce the photocatalytic activity, since the electrons cannot reach the adsorbed oxygen or dye on the catalyst surface efficiently [14,53].

Upon chlorophyll loading, the PL intensity of Chl/P25 was also lower than that of P25, indicating charge transfer between chlorophyll and P25 [56]. Due to the higher oxidation potential of the chlorophyll excited states, electrons can transfer from the chlorophyll excited states to the TiO_2 conduction band [1,57]. As a result, chlorophyll may potentially act as an electron donor, facilitating photocatalytic activity.

Table 2
Pseudo first-order kinetic rate constant (k), regression coefficient (R^2), and percentage of RhB degradation under visible light irradiation.

Catalysts	k (10^{-3} min^{-1})	R^2	Adsorption (%)	Degradation (%)
None	2.0 ± 0.2	0.89	-	14.4
P25	6.2 ± 0.2	0.99	1.2	41.1
Au_{25}/P25 (uc)	13.9 ± 0.2	1.00	8.4	73.4
Au_{25}/P25	10.4 ± 0.5	0.98	12.5	64.4
Au_{DP}/P25	3.6 ± 0.1	0.99	8.0	27.2
$Au_{6\ nm}$/P25	2.7 ± 0.1	0.99	8.5	22.4
$Au_{17\ nm}$/P25	2.8 ± 0.1	0.99	9.8	21.3
Chl/P25	33.1 ± 3.3	0.91	13.7	98.3
Chl-Au_{25}/P25 (uc)	102.0 ± 11.6	0.92	15.0	100
Chl-Au_{25}/P25	66.7 ± 4.0	0.97	19.2	99.8

Loading P25 with Au_{25} as well as chlorophyll (Fig. 6) therefore further lowers the PL intensity, significantly suppressing electron-hole pair recombination in the catalysts. The better charge separation efficiency should then lead to superior photodegradation activity as well.

3.5. Photocatalytic performance of chlorophyll-modified Au-functionalized TiO_2 catalysts

The photoactivities of the chlorophyll and/or Au-functionalized P25 catalysts are shown in Fig. 7. Prior to the photocatalytic performance test, a blank experiment was performed in the absence of a photocatalyst. This indicated a very slow direct photolysis of RhB (14.36% at 90 min). In addition, in the presence of photocatalysts but in the dark, RhB did not decompose even within 20 h.

Upon visible-light irradiation, the degradation efficiency of photocatalysts increased significantly, with up to 73% decomposition in 90 min for Au_{25}/P25 (uc) (Fig. 7(A)). Among all the Au/P25 catalysts, the Au_{25}/P25 (uc) and Au_{25}/P25 enhanced the photocatalytic performance of P25 by factors of 1.23 and 1.32, respectively. In contrast, the Au NPs-functionalized catalysts (Au_{DP}/P25, $Au_{6\ nm}$/P25, $Au_{17\ nm}$/P25) showed even lower degradation efficiency than P25 (lowered by factors of 1.14–1.20) and seemed to simply continue dye adsorption. Apparently, only the Au_{25} clusters (both uncalcined and calcined) improved the photocatalytic performance of P25. Interestingly, the uncalcined (Au_{25}/P25 (uc)) catalyst with intact ligands exhibited even higher efficiency than the calcined catalyst (Au_{25}/P25).

Furthermore, the effect of chlorophyll modification was examined (Fig. 7(B)). The direct loading of chlorophyll *a* onto P25 increased the dye adsorption capacity even more than the Au_{25} clusters did, indicating an outstanding interaction of RhB with chlorophyll. In analogy to the adsorption capacity, the photodegradation performance of Chl/P25 was ~2.37 times higher than that of P25 alone. The Chl-Au_{25}/P25 (uc) and Chl-Au_{25}/P25 catalysts exhibited photodegradation activity 2.49–1.45 times higher than that of the single-loaded (only Chl or Au25) P25 catalysts, and 3.64–3.22 times higher than that of P25. The activities of the photocatalysts were in the order of: Chl-Au_{25}/P25 (uc) > Chl-Au_{25}/P25 > Chl/P25 > Au_{25}/P25 (uc) > Au_{25}/P25 > P25. These results clearly indicate that both the Au_{25} clusters and chlorophyll play important roles in dye adsorption and visible-light-driven photocatalytic photodegradation over the functionalized P25 catalysts.

Furthermore, the kinetic rate constants (k) were calculated from the slope in plots of $\ln(C_0/C)$ vs. irradiation time (Fig. S9 and Table 2). The high regression coefficients (R^2) confirmed the pseudo-first-order kinetics of RhB photocatalytic degradation, in good agreement with previous studies [33,58]. Among all photocatalysts, the Chl-Au_{25}/P25 (uc) catalyst exhibited the fastest degradation, with the highest kinetic rate (102.00×10^{-3} min^{-1}), which was 16.4, 7.3, and 3.1 times higher than that of P25, Au_{25}/P25 (uc), and Chl/P25 catalysts, respectively.

Overall, it should be noted that the charge separation of all Au functionalized P25 catalysts was better than that of P25, specifically for

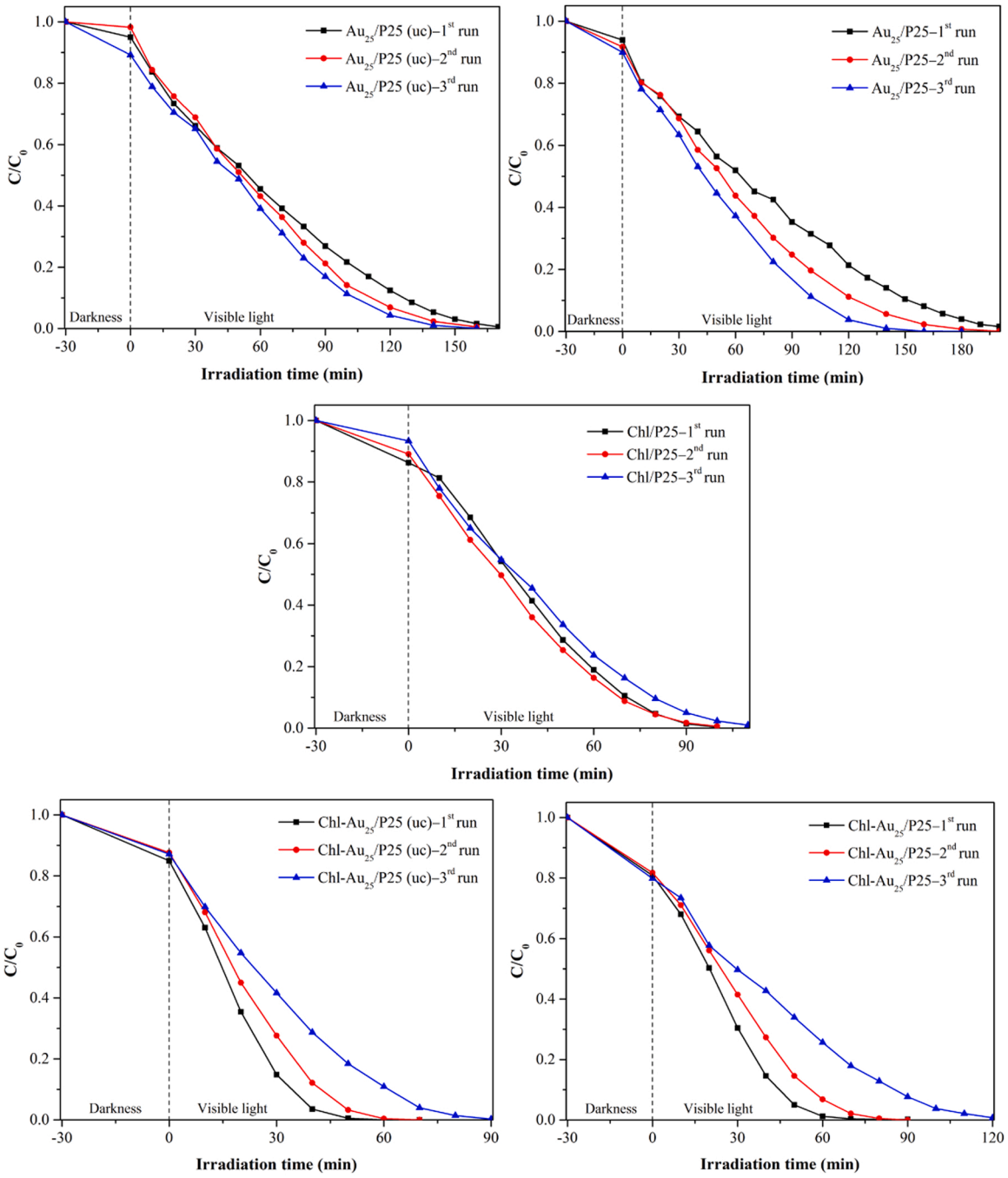

Fig. 8. Repeated photocatalytic degradation of rhodamine B over Au_{25}/P25 (uc), Au_{25}/P25, Chl/P25, Chl-Au_{25}/P25 (uc), and Chl-Au_{25}/P25 catalysts.

Au_{DP}/P25 and $Au_{6\ nm}$/P25 (cf. PL intensities in Fig. S8). However, for $Au_{17\ nm}$/P25, the large Au particle size disfavored photocatalytic activity, since the electrons cannot easily reach the adsorbed oxygen or dye on the catalyst surface [14,53]. Regarding the lower degradation efficiency of Au NPs-functionalized catalysts despite relatively small particle size (Au_{DP}/P25 and $Au_{6\ nm}$/P25), this may potentially be due to electronic quantum size effects changing the HOMO–LUMO energy gap, in contrast to the continuous conduction band of metallic Au NPs [14, 37,59].

In addition, the photodegradation efficiency of Au/P25 catalysts may not only depend on the Au cluster/particle size, but also on the atomic structure. The Au_{25} clusters of 1.4 nm size showed much better performance than Au_{DP}/P25, $Au_{6\ nm}$/P25, and $Au_{17\ nm}$/P25, although Au_{DP} were only slightly larger (2 nm). Apart from their size (1.4 nm), the Au_{25} clusters exhibit icosahedral atom-packing, different from the face-centered cubic (fcc) structure of Au nanoparticles [14,53]. The higher photodegradation efficiency of Au_{25}/P25 (uc) is thus potentially attributed to the icosahedral structure of the Au_{25} clusters [53,59–61].

With respect to the Au_{25}/P25 catalyst, after calcination at 400 °C the thiolate ligands were partially removed from the Au_{25} clusters, as can be seen from the significant decrease in the Au–S bond in the respective EXAFS spectrum of Chl-Au_{25}/P25 (Fig. S4). Creating clean Au surfaces was, however, accompanied by cluster growth (Fig. 1(b, c) and the calculations based on UV–vis spectra in Fig. S1). This partly counterbalanced the favorable Au cluster properties, leading to larger Au particles, but some Au_{25} clusters and ligands were likely maintained. In addition, the XPS results (Fig. S5(a,b)) also evidently indicated the coexistence of metallic Au in the electron-rich core and partially

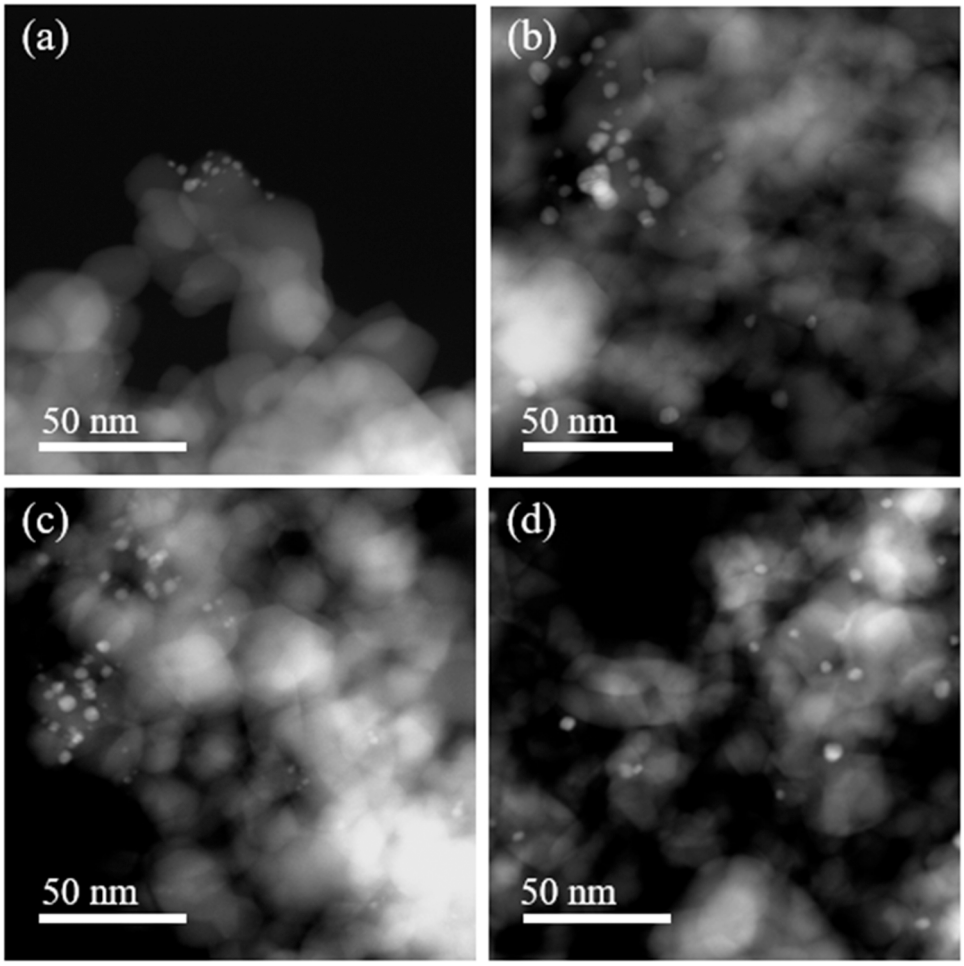

Fig. 9. STEM images of used catalysts: (a) Au_{25}/P25 (uc), (b) Au_{25}/P25, (c) Chl-Au_{25}/P25 (uc), and (d) Chl-Au_{25}/P25.

oxidized Au in the electron-deficient shell of thiolate-protected Au_{25} clusters. This suggests that the ligand shell of Au_{25} clusters plays an important role in the photocatalytic reaction, as the thiolate-protected Au_{25} clusters exhibited higher photocatalytic activity than the calcined Chl-Au_{25}/P25 catalyst [14,34,59].

Additional modification the $Au_{25}(SR)_{18}$-functionalized TiO_2 with chlorophyll *a*, i.e., creating chlorophyll modified Au_{25}-functionalized P25 (Chl-Au_{25}/P25 (uc) and Chl-Au_{25}/P25) led to outstanding absorption properties (Fig. 5 and Fig. S7). These results explain the excellent visible-light-driven photocatalytic activity of Chl-Au_{25}/P25 catalysts as they are able to utilize visible light to generate more photo-induced charges for the surface redox reactions.

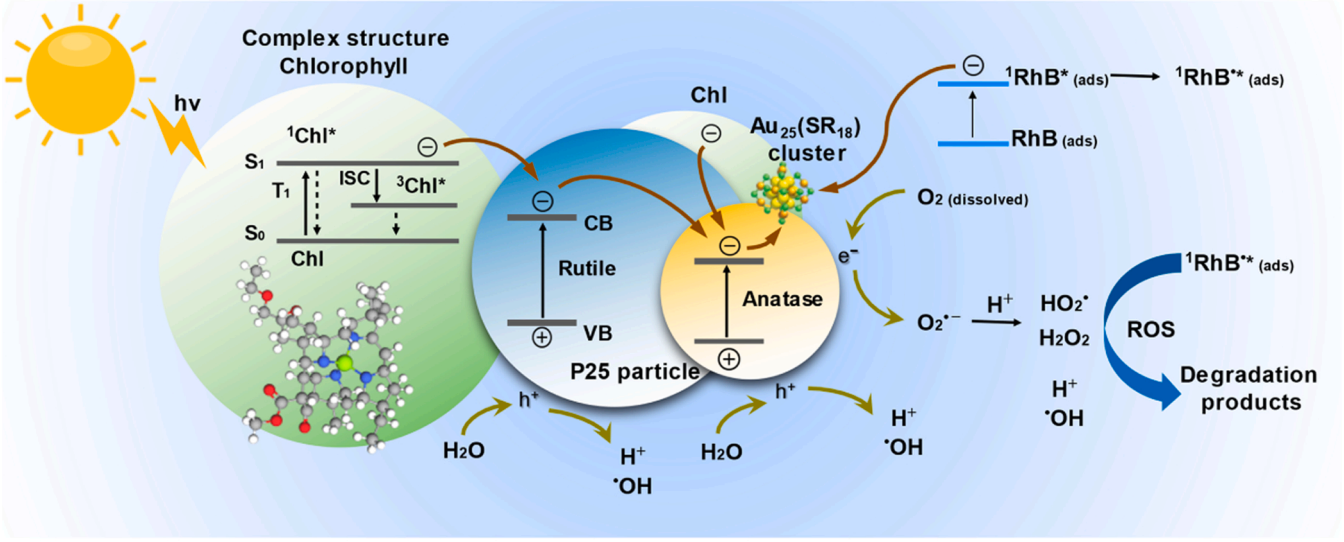

Fig. 10. Proposed mechanism for photocatalytic degradation of rhodamine B on chlorophyll-modified Au_{25}-functionalized P25 catalyst.

3.6. Reusability of Chl-Au_{25}/P25 catalysts

As catalyst reusability is very important for practical applications, the Au_{25}/P25 (uc), Au_{25}/P25, Chl/P25, Chl-Au_{25}/P25 (uc), and Chl-Au_{25}/P25 catalysts were tested for recycling performance (Fig. 8). After each experiment, the catalysts were collected by high-speed centrifugation and dried at 60 °C for 12 h before performing repeated runs under the same conditions. Interestingly, the dye adsorption, photocatalytic activity, and kinetic rate of Au_{25}/P25 (uc) and Au_{25}/P25 catalysts increased after each run, while those of all chlorophyll-loaded catalyst decreased. According to our previous study [1], the latter is likely due to the leaching of Mg from chlorophyll, lowering the photosensitizing activity of chlorophyll *a*.

In more detail, the kinetic rates of Au_{25}/P25 (uc) and Au_{25}/P25 catalysts were found to increase by factors of 2.2 and 1.4 upon three repeated experiments, respectively, pointing to high recyclability of the catalysts. STEM images of the used catalysts (Fig. 9) indicated that after three repeated experiments, the mean Au sizes in Au_{25}/P25 (uc) had increased from 1.4 to 1.7 nm, and in Au_{25}/P25 catalysts from 4.2 to 4.6 nm. The rate increase may thus be due to a successive (partial) removal of thiol ligands, creating more active Au surface.

In contrast, the kinetic rates of Chl/P25, Chl-Au_{25}/P25 (uc), and Chl-Au_{25}/P25 catalysts decreased 1.2, 2.1 and 2.3 times upon three repeated experiments, respectively. This was probably due to the gradual degradation of chlorophyll *a* on the used Au-functionalized P25 catalysts as evidenced by the FTIR spectra (Fig. S10), originating from the C═O stretching in conjugated ketone and carbonyl groups at 1600 cm^{-1} [40,41,62].

3.7. Proposed reaction mechanism over chlorophyll-modified $Au_{25}(SR)_{18}$-functionalized TiO_2 catalysts

Regarding the degradation of RhB over a series of chlorophyll-modified $Au_{25}(SR)_{18}$-functionalized TiO_2 catalysts, both chlorophyll and Au_{25} simultaneously enhance the P25 activity (Fig. 7(B), S9), resulting from deposition of chlorophyll onto the icosahedral Au_{25} clusters supported on P25 [34,50]. A schematic of the reaction mechanism of photocatalytic RhB degradation is presented in Fig. 10, illustrating charge separation and transfer.

Under visible light irradiation, RhB absorbs photons of visible light which accelerates electron transfer from a ground state to an excited state (^{1}RhB*). Simultaneously, chlorophyll (Chl) bonded to $Au_{25}(SR)_{18}$ nanoclusters and bound to both anatase and rutile phases of P25, similarly absorbs photons exciting electrons to an excited singlet state (1Chl*), where some electrons undergo intersystem crossing (ISC) to the triplet state (3Chl*). The electrons can transfer to the conduction band (CB) of P25 from both the excited states of RhB (^{1}RhB*) and chlorophyll (^{1}Chl*). As a result, ^{1}RhB•* molecular ion radicals and a cationic form of chlorophyll on the P25 surface are formed. In addition, the anatase and rutile phases of P25 can generate electron-hole pairs by absorbing photons with energy equal to or higher than their band gap energy. Consequently, the electrons in the conduction band of P25 react with adsorbed oxygen to form a superoxide radical (O_2•−), while the holes in the P25 valence band (VB) react with surface water or hydroxyl groups to form reactive oxygen species (ROS: hydroxyl radical (•OH) or hydroperoxyl radical (HO_2•), and hydrogen peroxide (H_2O_2)). These highly reactive radical species then react with RhB molecules, completing the RhB degradation cycle. As electrons move to P25 particles, the chlorophyll molecules then regain the missing electrons from electron donor molecules through an electron carrier in the electron transport chain in the chlorophyll structure [63,64]. Accordingly, better photodegradation performance was evidently observed.

4. Conclusion

In this work, to improve the light harvesting properties of photocatalysts, a series of Au functionalized P25 (Au_{25} clusters and Au nanoparticles (NPs)) and chlorophyll-modified Au functionalized P25 (Chl-Au_{25}/P25 (uc; with thiol ligands) and Chl-Au_{25}/P25) catalysts have been successfully prepared and examined in RhB photodegradation. Under visible light irradiation, the activities of the photocatalysts are in the order of: Chl-Au_{25}/P25 (uc) > Chl-Au_{25}/P25 > Chl/P25 > Au_{25}/P25 (uc) > Au_{25}/P25 > P25 > Au_{DP}/P25 > $Au_{6\ nm}$/P25, $Au_{17\ nm}$/P25. The results clearly indicated that the visible-light absorption of Chl-Au_{25}/P25 (uc) and Chl-Au_{25}/P25 catalysts was significantly stronger than that of catalysts loaded by either Au_{25} or chlorophyll. Moreover, the presence of both Au_{25} and chlorophyll simultaneously enhanced the P25 activity due to the deposition of chlorophyll onto the icosahedral Au_{25} clusters supported by P25, lowering the PL intensity, significantly suppressing electron-hole pair recombination in the catalysts. This led to better charge separation efficiency and superior photodegradation activity. Using a chlorophyll-modified $Au_{25}(SR)_{18}$-functionalized P25 catalyst, the degradation rate of RhB was approximately 16 times higher than that of P25.

CRediT authorship contribution statement

Thanaree Phongamwong: Investigation, Writing – orignal draft. **Noelia Barrabés:** Supervision, Validation, Data curation. **Waleeporn Donphai:** Validation, Data curation. **Thongthai Witoon:** Validation, Data curation. **Günther Rupprechter:** Conceptualization, Supervision, Writing – review & editing. **Metta Chareonpanich:** Conceptualization, Supervision, Writing – review & editing.

Declaration of Competing Interest

The authors declare that they have no known competing financial interests or personal relationships that could have appeared to influence the work reported in this paper.

Data Availability

No data was used for the research described in the article.

Acknowledgements

This work was financially supported by grants from the National Research Council of Thailand (NRCT) through the Research Team Promotion Grant/Senior Research Scholar (Grant No. N42A640324); the Kasetsart University Research and Development Institute (KURDI) and by the Austrian Science Fund (FWF) via the Doctoral School DK+ Solids4Fun (W1243) and SFB TACO (F81-P08).

Appendix A. Supporting information

Supplementary data associated with this article can be found in the online version at doi:10.1016/j.apcatb.2022.122336.

References

[1] T. Phongamwong, W. Donphai, P. Prasitchoke, C. Rameshan, N. Barrabeís, W. Klysubun, G. Rupprechter, M. Chareonpanich, Novel visible-light-sensitized Chl-Mg/P25 catalysts for photocatalytic degradation of rhodamine B, Appl. Catal. B Environ. 207 (2017) 326–334.
[2] T. Phongamwong, M. Chareonpanich, J. Limtrakul, Role of chlorophyll in Spirulina on photocatalytic activity of CO_2 reduction under visible light over modified N-doped TiO_2 photocatalysts, Appl. Catal. B Environ. 168 (2015) 114–124.
[3] C. Worathitanon, K. Jangyubol, P. Ruengrung, W. Donphai, W. Klysubun, N. Chanlek, P. Prasitchoke, M. Chareonpanich, High performance visible-light responsive Chl-Cu/ZnO catalysts for photodegradation of rhodamine B, Appl. Catal. B Environ. 241 (2019) 359–366.
[4] J. Nie, J. Schneider, F. Sieland, L. Zhou, S. Xia, D.W. Bahnemann, New insights into the surface plasmon resonance (SPR) driven photocatalytic H_2 production of Au–TiO_2, RCS Adv. 8 (46) (2018) 25881–25887.

[5] Y. Gao, W. Nie, Q. Zhu, X. Wang, S. Wang, F. Fan, C. Li, The polarization effect in surface-plasmon-induced photocatalysis on Au/TiO_2 nanoparticles, Angew. Chem. 132 (41) (2020) 18375–18380.

[6] S. Zeng, E. Vahidzadeh, C.G. VanEssen, P. Kar, R. Kisslinger, A. Goswami, Y. Zhang, N. Mahdi, S. Riddell, A.E. Kobryn, S. Gusarov, Optical control of selectivity of high rate CO_2 photoreduction via interband-or hot electron Z-scheme reaction pathways in Au-TiO_2 plasmonic photonic crystal photocatalyst, Appl. Catal. B Environ. 267 (2020), 118644.

[7] Y. Kim, J.G. Smith, P.K. Jain, Harvesting multiple electron–hole pairs generated through plasmonic excitation of Au nanoparticles, Nat. Chem. 10 (7) (2018) 763–769.

[8] S. Mao, J.W. Shi, G. Sun, D. Ma, C. He, Z. Pu, K. Song, Y. Cheng, Au nanodots@ thiol-UiO66@ $ZnIn_2S_4$ nanosheets with significantly enhanced visible-light photocatalytic H_2 evolution: the effect of different Au positions on the transfer of electron-hole pairs, Appl. Catal. B Environ. 282 (2021), 119550.

[9] T. Kawawaki, Y. Negishi, H. Kawasaki, Photo/electrocatalysis and photosensitization using metal nanoclusters for green energy and medical applications, Nanoscale Adv. 2 (1) (2020) 17–36.

[10] D. Hikisou, S. Saita, S. Miyata, H. Miyaji, T. Furuike, H. Tamura, H. Kawasaki, Aggregation/self-assembly-induced approach for efficient Au-Ag bimetallic nanocluster-based photosensitizers, J. Phys. Chem. C. 122 (23) (2018) 12494–12501.

[11] B. Weng, K.Q. Lu, Z. Tang, H.M. Chen, Y.J. Xu, Stabilizing ultrasmall Au clusters for enhanced photoredox catalysis, Nat. Commun. 9 (1) (2018) 1–11.

[12] A. Sels, G. Salassa, S. Pollitt, C. Guglieri, G. Rupprechter, N. Barrabés, T. Bürgi, Structural Investigation of the ligand exchange reaction with rigid dithiol on doped (Pt, Pd) $Au_{2,\ 5}$ Clust., J. Phys. Chem. C. 121 (2017) 10919–10926.

[13] Y. Negishi, T. Nakazaki, S. Malola, S. Takano, Y. Niihori, W. Kurashige, H. Häkkinen, A critical size for emergence of nonbulk electronic and geometric structures in dodecanethiolate-protected Au clusters, J. Am. Chem. Soc. 137 (3) (2015) 1206–1212.

[14] G. Li, R. Jin, Atomically precise gold nanoclusters as new model catalysts, Acc. Chem. Res. 46 (8) (2013) 1749–1758.

[15] B. Zhang, A. Sels, G. Salassa, S. Pollitt, V. Truttmann, C. Rameshan, J. Llorca, W. Olszewski, G. Rupprechter, T. Bürgi, N. Barrabés, Ligand migration from cluster to support: a crucial factor for catalysis by thiolate-protected gold clusters, ChemCatChem 10 (23) (2018) 5372–5376.

[16] S. Pollitt, V. Truttmann, T. Haunold, C. Garcia, W. Olszewski, J. Llorca, N. Barrabés, G. Rupprechter, The dynamic structure of $Au_{38}(SR)_{24}$ nanoclusters supported on CeO_2 upon pretreatment and CO oxidation, ACS Catal. 10 (11) (2020) 6144–6148.

[17] K.D.M. Weerawardene, C.M. Aikens, Theoretical insights into the origin of photoluminescence of $Au_{25}(SR)^{-}_{18}$ nanoparticles, J. Am. Chem. Soc. 138 (35) (2016) 11202–11210.

[18] K.R. Krishnadas, A. Ghosh, A. Baksi, I. Chakraborty, G. Natarajan, T. Pradeep, Intercluster reactions between $Au_{25}(SR)_{18}$ and $Ag_{44}(SR)_{30}$, J. Am. Chem. Soc. 138 (1) (2016) 140–148.

[19] V. Truttmann, H. Drexler, M. Stöger-Pollach, T. Kawawaki, Y. Negishi, N. Barrabés, G. Rupprechter, CeO_2 supported gold nanocluster catalysts for CO oxidation: surface evolution influenced by the ligand shell, ChemCatChem 14 (14) (2022), e202200322.

[20] C. Garcia, V. Truttmann, I. Lopez, T. Haunold, C. Marini, C. Rameshan, E. Pittenauer, P. Kregsamer, K. Dobrezberger, M. Stöger-Pollach, N. Barrabés, Dynamics of Pd dopant atoms inside Au nanoclusters during catalytic CO oxidation, J. Phys. Chem. C. 124 (43) (2020) 23626–23636.

[21] G. Rupprechter, Operando surface spectroscopy and microscopy during catalytic reactions: from clusters via nanoparticles to meso-scale aggregates, Small 17 (27) (2021) 2004289.

[22] C. García, S. Pollitt, M. van der Linden, V. Truttmann, C. Rameshan, R. Rameshan, E. Pittenauer, G. Allmaier, P. Kregsamer, M. Stöger-Pollach, N. Barrabés, Support effect on the reactivity and stability of $Au_{25}(SR)_{18}$ and $Au_{144}(SR)_{60}$ nanoclusters in liquid phase cyclohexane oxidation, Catal. Today 336 (2019) 174–185.

[23] M. Zhu, E. Lanni, N. Garg, M.E. Bier, R. Jin, Kinetically controlled, high-yield synthesis of Au_{25} clusters, J. Am. Chem. Soc. 130 (4) (2008) 1138–1139.

[24] C. Liu, G. Li, G. Pang, R. Jin, Toward understanding the growth mechanism of $Au_n(SR)_m$ nanoclusters: effect of solvent on cluster size, RSC Adv. 3 (25) (2013) 9778–9784.

[25] S. Zhang, X.S. Li, B. Zhu, J.L. Liu, X. Zhu, A.M. Zhu, B.W.L. Jang, Atmospheric-pressure O_2 plasma treatment of Au/TiO_2 catalysts for CO oxidation, Catal. Today 256 (2015) 142–147.

[26] Y. Wang, X. Ma, Y. Wen, Y. Xing, Z. Zhang, H. Yang, Direct electrochemistry and bioelectrocatalysis of horseradish peroxidase based on gold nano-seeds dotted TiO_2 nanocomposite, Biosens. Bioelectron. 25 (11) (2010) 2442–2446.

[27] W. Haiss, N.T. Thanh, J. Aveyard, D.G. Fernig, Determination of size and concentration of gold nanoparticles from UV− Vis spectra, Anal. Chem. 79 (11) (2007) 4215–4221.

[28] U. Cataldi, R. Caputo, Y. Kurylyak, G. Klein, M. Chekini, C. Umeton, T. Bürgi, Growing gold nanoparticles on a flexible substrate to enable simple mechanical control of their plasmonic coupling, J. Mater. Chem. C. 2 (37) (2014) 7927–7933.

[29] A. Bennett, L. Bogorad, Complementary chromatic adaptation in a filamentous blue-green alga, J. Cell Biol. 58 (1973) 419–435.

[30] R.A. Monteiro, S.M. Miranda, V.J. Vilar, L.M. Pastrana-Martínez, P.B. Tavares, R. A. Boaventura, J.L. Faria, E. Pinto, A.M. Silva, N-modified TiO_2 photocatalytic activity towards diphenhydramine degradation and Escherichia coli inactivation in aqueous solutions, Appl. Catal. B Environ. 162 (2015) 66–74.

[31] D. Li, Q. Zhu, C. Han, Y. Yang, W. Jiang, Z. Zhang, Photocatalytic degradation of recalcitrant organic pollutants in water using a novel cylindrical multi-column photoreactor packed with TiO_2-coated silica gel beads, J. Hazard. Mater. 285 (2015) 398–408.

[32] M. El-Kemary, H. El-Shamy, I. El-Mehasseb, Photocatalytic degradation of ciprofloxacin drug in water using ZnO nanoparticles, J. Lumin 130 (12) (2010) 2327–2331.

[33] K. Natarajan, T.S. Natarajan, H.C. Bajaj, R.J. Tayade, Photocatalytic reactor based on UV-LED/TiO_2 coated quartz tube for degradation of dyes, Chem. Eng. J. 178 (2011) 40–49.

[34] C. Yu, G. Li, S. Kumar, H. Kawasaki, R. Jin, Stable Au_25(SR)18/TiO2 composite nanostructure with enhanced visible light photocatalytic activity, J. Phys. Chem. Lett. 4 (17) (2013) 2847–2852.

[35] Z. Wu, J. Chen, R. Jin, One-Pot Synthesis of $Au_{25}(SG)_{18}$ 2–and 4–nm gold nanoparticles and comparison of their size-dependent properties, Adv. Funct. Mater. 21 (1) (2011) 177–183.

[36] W. Li, Q. Ge, Oxide-supported $Au_n(SR)_m$ nanoclusters for CO oxidation, Chin. J. Catal. 36 (2) (2015) 135–138.

[37] O. Lopez-Acevedo, K.A. Kacprzak, J. Akola, H. Häkkinen, Quantum size effects in ambient CO oxidation catalysed by ligand-protected gold clusters, Nat. Chem. 2 (4) (2010) 329–334.

[38] S. Gaur, J.T. Miller, D. Stellwagen, A. Sanampudi, C.S. Kumar, J.J. Spivey, Synthesis, characterization, and testing of supported Au catalysts prepared from atomically-tailored $Au_{38}(SC_{12}H_{25})_{24}$ clusters, Phys. Chem. Chem. Phys. 14 (5) (2012) 1627–1634.

[39] M. Farrag, M. Tschurl, A. Dass, U. Heiz, Infra-red spectroscopy of size selected Au_{25}, Au_{38} and Au_{144} ligand protected gold clusters, Phys. Chem. Chem. Phys. 15 (30) (2013) 12539–12542.

[40] F. Xu, Q.A. Zhou, J.Z. Sun, C.F. Liu, J.L. Ren, R.C. Sun, S. Curling, P. Fowler, M. S. Baird, Fractionation and characterization of chlorophyll and lignin from de-juiced Italian ryegrass (Lolium multifolrum) and timothy grass (Phleum pratense), Process Biochem 42 (5) (2007) 913–918.

[41] Z. Mehraban, F. Farzaneh, A. Shafiekhani, Synthesis and characterization of a new organic–inorganic hybrid NiO–chlorophyll-a as optical material, Opt. Mater. 29 (8) (2007) 927–931.

[42] B. Zhang, S. Kaziz, H. Li, M.G. Hevia, D. Wodka, C. Mazet, T. Bürgi, N. Barrabés, Modulation of active sites in supported $Au_3$8(SC2H4Ph)24 cluster catalysts: effect of atmosphere and support material, J. Phys. Chem. C. 119 (20) (2015) 11193–11199.

[43] A. Shivhare, K.E. Lee, Y. Hu, R.W. Scott, Following the Reactivity of $Au_{25}(SC_8H_9)^{-}_{18}$Clusters with Pd^{2+} and Ag^{+} ions using in situ X-ray absorption spectroscopy: a tale of two metals, J. Phys. Chem. 119 (40) (2015) 23279–23284.

[44] Z. Luo, X. Yuan, Y. Yu, Q. Zhang, D.T. Leong, J.Y. Lee, J. Xie, From aggregation-induced emission of Au (I)–thiolate complexes to ultrabright Au (0)@ Au (I)–thiolate core–shell nanoclusters, J. Am. Chem. Soc. 134 (40) (2012) 16662–16670.

[45] S. Benjamin, D. Vaya, P.B. Punjabi, S.C. Ameta, Enhancing photocatalytic activity of zinc oxide by coating with some natural pigments, Arab. J. Chem. 4 (2) (2011) 205–209.

[46] S. Peters, S. Peredkov, M. Neeb, W. Eberhardt, M. Al-Hada, Size-dependent XPS spectra of small supported Au-clusters, Surf. Sci. 608 (2013) 129–134.

[47] G. Pramanik, J. Humpolickova, J. Valenta, P. Kundu, S. Bals, P. Bour, P. Cigler, Gold nanoclusters with bright near-infrared photoluminescence, Nanoscale 10 (2018) 3792–3798.

[48] D. Zhang, M. Wen, S. Zhang, P. Liu, W. Zhu, G. Li, H. Li, Au nanoparticles enhanced rutile TiO_2 nanorod bundles with high visible-light photocatalytic performance for NO oxidation, Appl. Catal. B Environ. 147 (2014) 610–616.

[49] A. Rismanchian, Y.W. Chen, S.S. Chuang, In situ infrared study of photoreaction of ethanol on Au and Ag/TiO_2, Catal. Today 264 (2016) 16–22.

[50] J.O. Méndez, C.R. López, E.P. Melián, O.G. Díaz, J.D. Rodríguez, D.F. Hevia, M. Macías, Production of hydrogen by water photo-splitting over commercial and synthesised Au/TiO_2 catalysts, Appl. Catal. B Environ. 147 (2014) 439–452.

[51] A.G. Dosado, W.T. Chen, A. Chan, D. Sun-Waterhouse, G.I. Waterhouse, Novel Au/TiO_2 photocatalysts for hydrogen production in alcohol–water mixtures based on hydrogen titanate nanotube precursors, J. Catal. 330 (2015) 238–254.

[52] O. Rosseler, M.V. Shankar, M. Karkmaz-Le Du, L. Schmidlin, N. Keller, V. Keller, Solar, light photocatalytic hydrogen production from water over Pt and Au/TiO_2 (anatase/rutile) photocatalysts: influence of noble metal and porogen promotion, J. Catal. 269 (1) (2010) 179–190.

[53] Á. Kmetykó, K. Mogyorósi, P. Pusztai, T. Radu, Z. Kónya, A. Dombi, K. Hernádi, Photocatalytic H_2 evolution using different commercial TiO_2 catalysts deposited with finely size-tailored au nanoparticles: Critical dependence on au particle size, Materials 7 (12) (2014) 7615–7633.

[54] T. Hanžić, A. Jurkin, M. Maksimović, Gotić, The synthesis of gold nanoparticles by a citrate-radiolytical method, Radiat. Phys. Chem. 106 (2015) 77–82.

[55] S. Sun, J. Ding, J. Bao, C. Gao, Z. Qi, X. Yang, B. He, C. Li, Photocatalytic degradation of gaseous toluene on Fe-TiO_2 under visible light irradiation: a study on the structure, activity and deactivation mechanism, Appl. Surf. Sci.. 258 (12) (2012) 5031–5037.

[56] H. Hagiwara, T. Inoue, K. Kaneko, T. Ishihara, Charge-transfer mechanism in Pt/$KTa(Zr)O_3$ photocatalysts modified with porphyrinoids for water splitting, Chem. Eur. J. 15 (46) (2009) 12862–12870.

[57] A. Kathiravan, M. Chandramohan, R. Renganathan, S. Sekar, Cyanobacterial chlorophyll as a sensitizer for colloidal TiO_2, Spectrochim. Acta - Part A Mol. Biomol. Spectrosc. 71 (5) (2009) 1783–1787.

[58] J. Di, J. Xia, Y. Ge, H. Li, H. Ji, H. Xu, Q. Zhang, H. Li, M. Li, Novel visible-light-driven CQDs/Bi_2WO_6 hybrid materials with enhanced photocatalytic activity

toward organic pollutants degradation and mechanism insight, Appl. Catal. B Environ. 168 (2015) 51–61.
[59] Y. Zhu, R. Jin, Y. Sun, Atomically monodisperse gold nanoclusters catalysts with precise core-shell structure, Catalysts 1 (1) (2011) 3–17.
[60] Y. Zhu, H. Qian, M. Zhu, R. Jin, Thiolate-protected aun nanoclusters as catalysts for selective oxidation and hydrogenation processes, Adv. Mater. 22 (17) (2010) 1915–1920.
[61] Y. Zhu, H. Qian, R. Jin, An Atomic-Level Strategy for Unraveling Gold Nanocatalysis from the Perspective of Aun(SR)m Nanoclusters, Chem. Eur. J. 16 (37) 11455–11462.
[62] J.Y. Li, W.H. Ma, P.X. Lei, J.C. Zhao, Detection of intermediates in the TiO_2-assisted photodegradation of Rhodamine B under visible light irradiation, J. Environ. Sci. 19 (2007) 892–896.
[63] D.W. Lawlor, Photosynthesis: Molecular, Physiological and Environmental. Process, second ed., Longman Scientific & Technical, Essex, 1993, pp. 1–8.
[64] M.F. Hipkins, N.R. Baker, Photosynthesis: Energy Transduction: A Practical Approach, IRL Press Limited, Oxford, Washington D.C., 1986, pp. 1–15.